HORN ANTENNAS

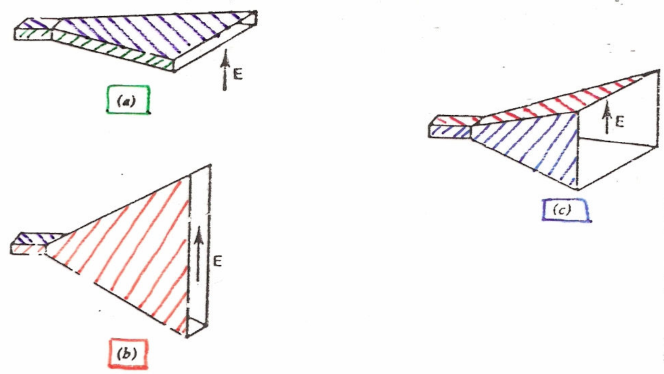

Figure – Rectangular horn antennas. (a) H-plane sectoral horn. (b) E-plane sectoral horn. (c) Pyramidal horn.

H-PLANE SECTORAL HORN

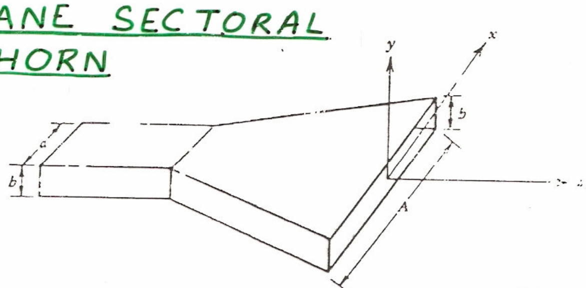

TOP VIEW

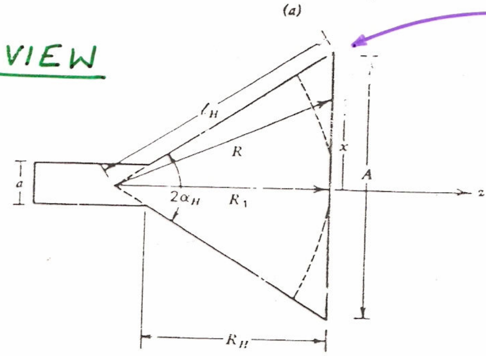

Phase error

$$\delta = \frac{\beta}{2R_1} x^2$$

$$\delta_{max} = \frac{\beta}{2R_1}\left(\frac{A}{2}\right)^2 = 2\pi \frac{A^2}{8\lambda R_1} = 2\pi t$$

Figure – H-plane sectoral horn antenna. (a) Overall geometry. (b) Cross section through the xz-plane (H-plane).

$$\ell_H^2 = R_1^2 + \left(\frac{A}{2}\right)^2, \quad \alpha_H = \tan^{-1}\left(\frac{A}{2R_1}\right)$$

TE$_{10}$ mode in waveguide

$$E_y = E_0 \cos\left(\frac{\pi x}{a}\right) e^{-j\beta_g z}$$

$$H_x = -E_y / Z_g, \quad Z_g = \eta\left[1 - \left(\frac{\lambda}{2a}\right)^2\right]^{-1/2}$$

Aperture phase variation

$$= e^{-j\beta(R-R_1)} \quad \text{in } x\text{-direction}$$

$$= \text{Constant} \quad \text{in } y\text{-} \quad "$$

$$R = \sqrt{R_1^2 + x^2} \approx R_1\left[1 + \frac{1}{2}\left(\frac{x}{R_1}\right)^2\right]$$

$$R - R_1 \simeq \frac{1}{2}\frac{x^2}{R_1}$$

Aperture field distribution

$$E_{ay} = E_0 \cos\frac{\pi x}{A} \, e^{-j(\beta/2R_1)x^2}$$

Phase error

$$\delta = \frac{\beta}{2R_1}x^2$$

$$\delta_{max} = \frac{\beta}{2R_1}\left(\frac{A}{2}\right)^2 = \frac{2\pi}{\lambda}\frac{A^2}{8R_1} = 2\pi t$$

$$t = \frac{A^2}{8\lambda R_1} = \frac{1}{8}\left(\frac{A}{\lambda}\right)^2\frac{1}{R_1/\lambda}$$

DIRECTIVITY CURVES

H-PLANE SECTORAL HORN

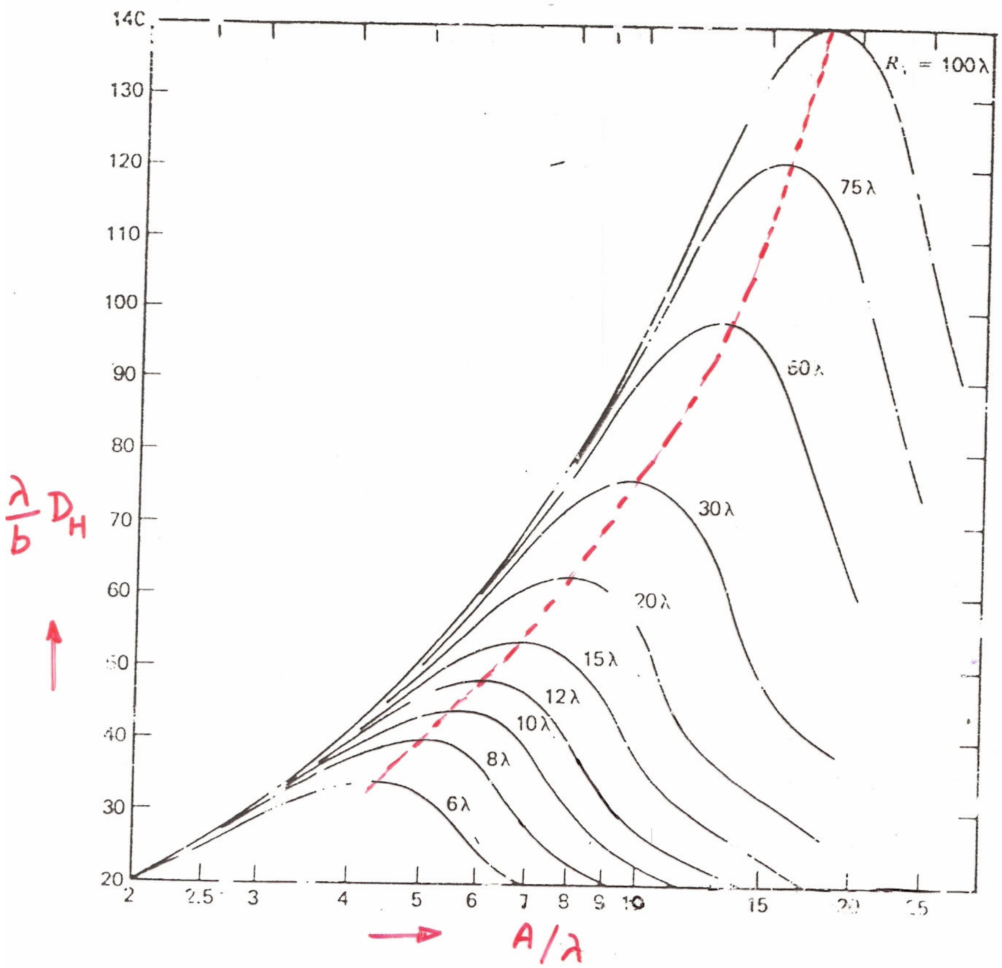

Figure — Universal directivity curves for an H-plane sectoral horn. For pyramidal horns the vertical axis values are $(\lambda/B)D_H$.

OPTIMUM GAIN

R_1	6	10	20	100
A	4.24	5.48	7.75	17.32

$$A = \sqrt{3\lambda R_1}$$

$$t_{opt} = \left.\frac{A^2}{8\lambda R_1}\right|_{A^2 = 3\lambda R_1} = \frac{3}{8}$$

$$\delta_{max} = 2\pi t = 2\pi\left(\frac{3}{8}\right) = \frac{3\pi}{4} = 135^\circ$$

Universal Radiation Pattern
H-plane sectoral horn

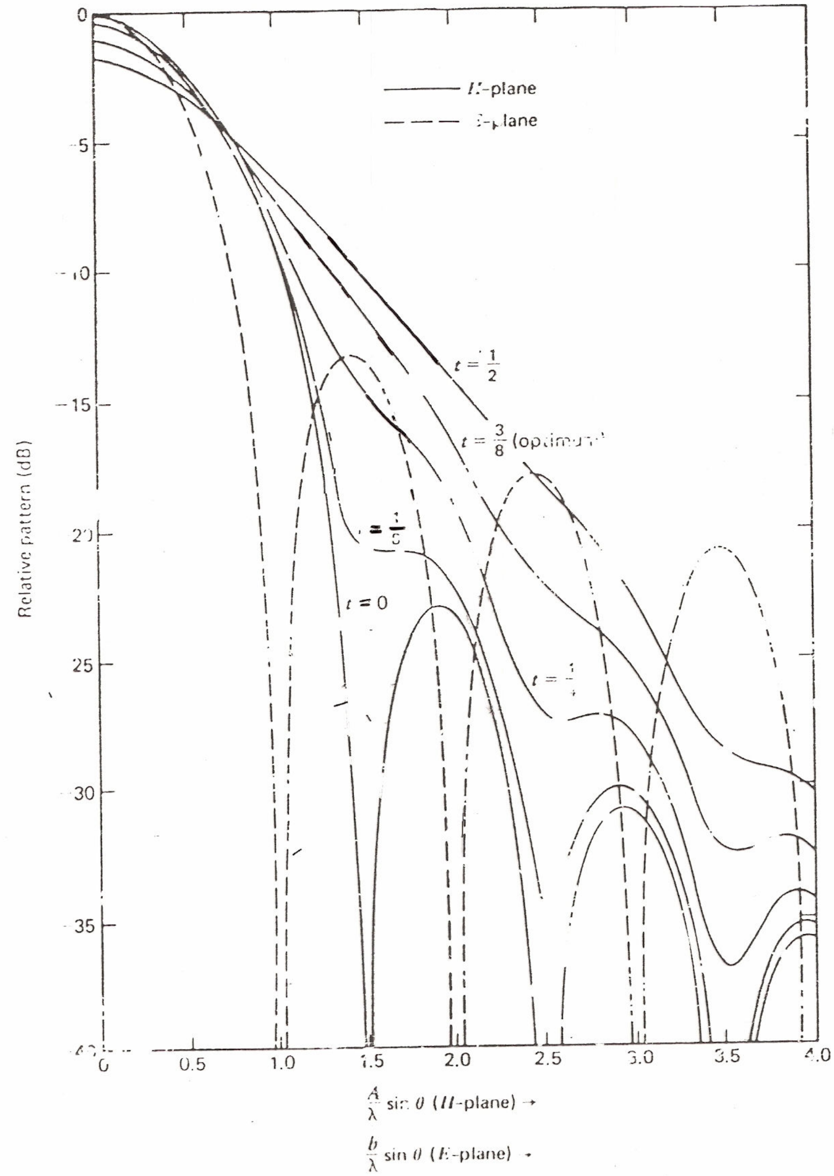

Figure – Universal radiation patterns for the principal planes of an H-plane sectoral horn as shown in Fig. 8-10. The factor $(1 + \cos\theta)/2$ is not included.

E-PLANE SECTORAL HORN

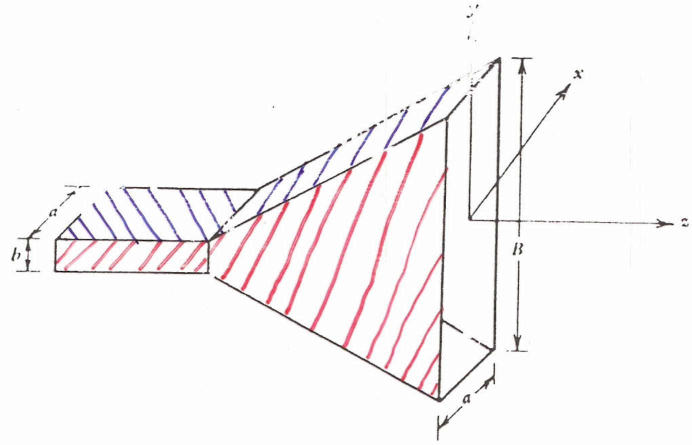

(a)

SIDE-VIEW

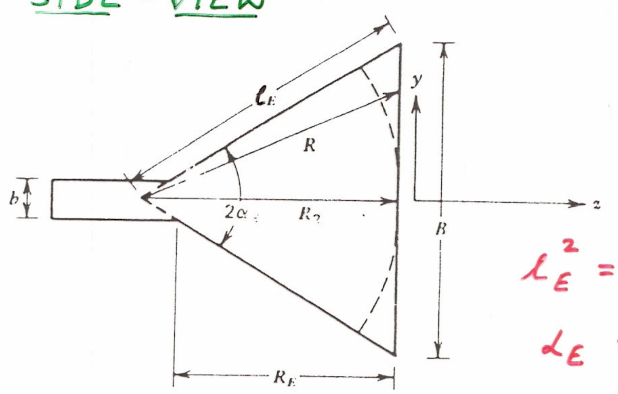

$$\ell_E^2 = R_2^2 + \left(\frac{B}{2}\right)^2$$

$$\alpha_E = \tan^{-1}\left(\frac{B}{2R_2}\right)$$

(b)

Figure — E-plane sectoral horn antenna. (a) Overall geometry. (b) Cross section through the yz-plane (E-plane).

Electric Field distribution

$$E_{ay} = E_0 \cos\frac{\pi x}{a}\, e^{-j(\beta/2R_2)y^2}$$

$$\delta = \frac{\beta}{2R_2} y^2 \Rightarrow \delta_{max} = 2\pi\left(\frac{B^2}{8\lambda R_2}\right) = 2\pi S$$

$$S = \frac{B^2}{8\lambda R_2} = \frac{1}{8}\left(\frac{B}{\lambda}\right)^2 \frac{1}{R_2/\lambda}$$

E-PLANE SECTORAL HORN

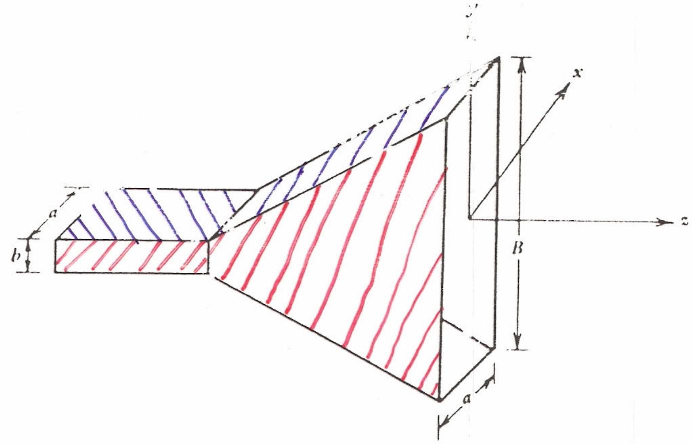

(a)

SIDE - VIEW

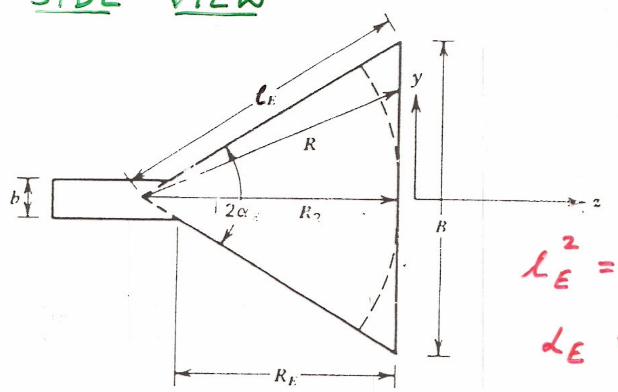

(b)

$$l_E^2 = R_2^2 + \left(\frac{B}{2}\right)^2$$

$$\alpha_E = \tan^{-1}\left(\frac{B}{2R_2}\right)$$

Figure — E-plane sectoral horn antenna. (a) Overall geometry. (b) Cross section through the yz-plane (E-plane).

Electric Field distribution

$$E_{ay} = E_0 \cos \frac{\pi x}{a} \, e^{-j(\beta/2R_2)y^2}$$

$$\delta = \frac{\beta}{2R_2} y^2 \Rightarrow \delta_{max} = 2\pi\left(\frac{B^2}{8\lambda R_2}\right) = 2\pi s$$

$$s = \frac{B^2}{8\lambda R_2} = \frac{1}{8}\left(\frac{B}{\lambda}\right)^2 \frac{1}{R_2/\lambda}$$

DIRECTIVITY CURVES

E - plane Sectoral Horn

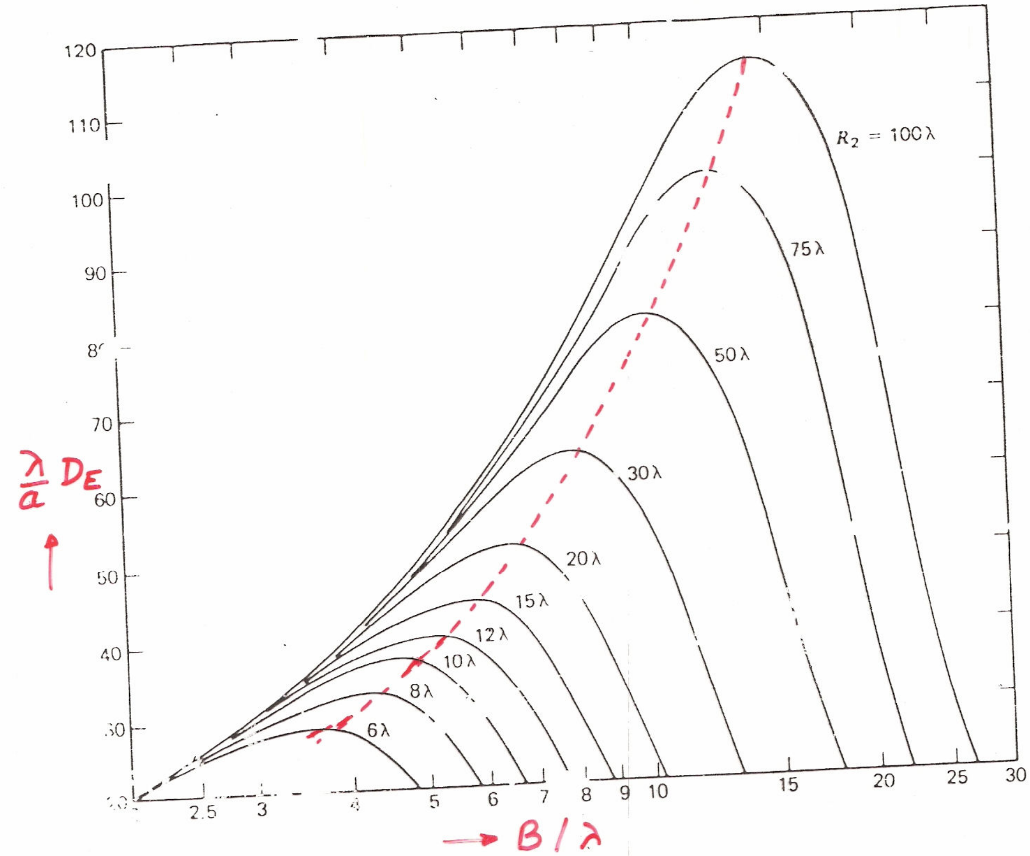

Figure — Universal directivity curves for an E-plane sectoral horn. For pyramidal horns the vertical axis values are $(\lambda/A)D_E$.

R_2	B
6	3.46
10	4.47
20	6.32
100	14.14

Optimum Directivity

$$B = \sqrt{2\lambda R_2}$$

$$S_{opt} = \frac{B^2}{8\lambda R_2} = \frac{1}{4}$$

$$\delta_{max} = 2\pi\, S_{opt} = \frac{\pi}{2} = 90^\circ$$

RADIATION PATTERN

E - Plane Sectoral Horn

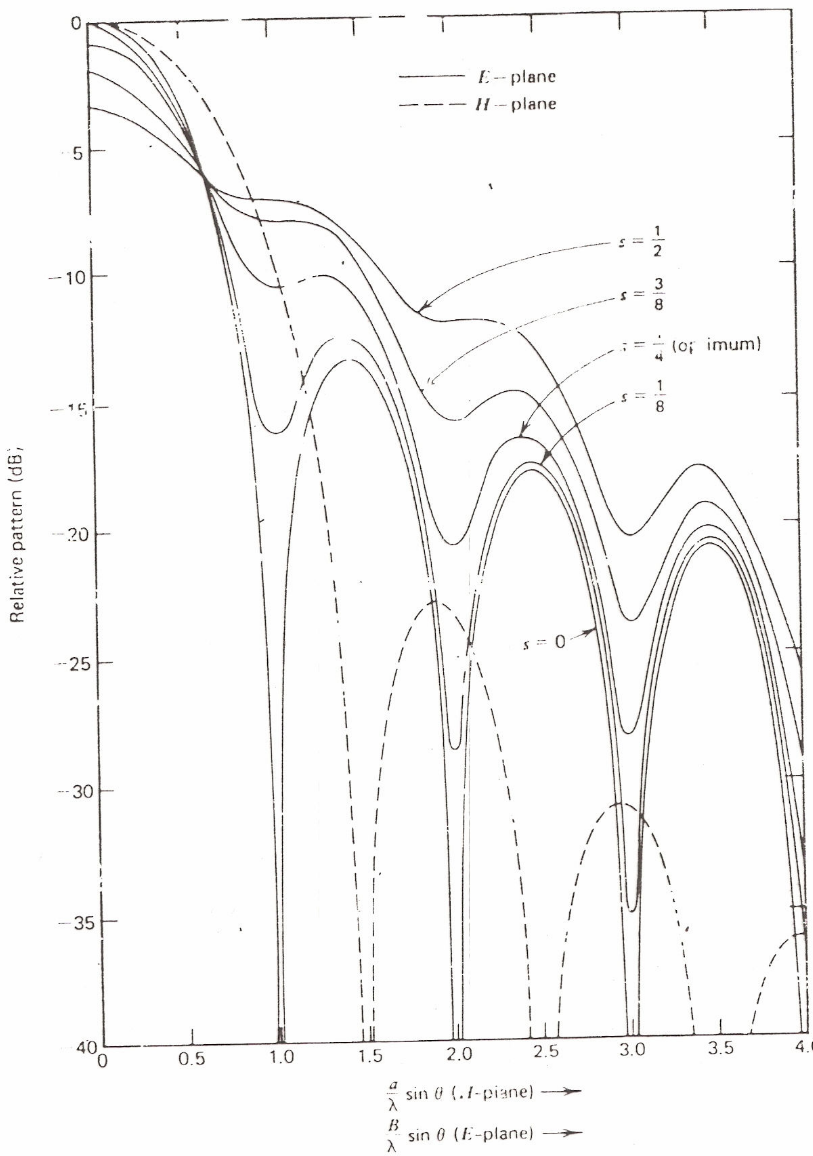

Figure – Universal radiation patterns for the principal planes of an E-plane sectoral horn antenna as shown in Fig. . The factor $(1 + \cos\theta)/2$ is not included.

PYRAMIDAL HORN DESIGN

$$A = \sqrt{3\lambda R_1} \approx \sqrt{3\lambda \ell_H} \quad - (1)$$

$$B = \sqrt{2\lambda R_2} \approx \sqrt{2\lambda \ell_E} \quad - (2)$$

Gain $G = \epsilon_{ap} \frac{4\pi}{\lambda^2} A_p$ $\quad (A_{eff} = \frac{1}{2} A_p)$

$$= \frac{1}{2} \frac{4\pi}{\lambda^2} AB = \frac{2\pi}{\lambda^2} AB \quad - (3)$$

For physical realization of horn

$$\boxed{R_E = R_H}$$

$$(B-b)\sqrt{\left(\frac{\ell_E}{B}\right)^2 - \frac{1}{4}} = (A-a)\sqrt{\left(\frac{\ell_H}{A}\right)^2 - \frac{1}{4}} \quad - (4)$$

From (1) - (4)

$$\left[\sqrt{2\sigma} - \frac{b}{\lambda}\right]^2 (2\sigma - 1) = \left(\frac{G}{2\sqrt{2}\,\pi} \frac{1}{\sqrt{\sigma}} - \frac{a}{\lambda}\right)^2 \left(\frac{G^2}{18\pi^2} \frac{1}{\sigma} - 1\right) \quad - (5)$$

$$\sigma = \ell_E / \lambda$$

Solve eqn. (5) iteratively

First trial $\sigma_1 = \frac{G}{2\pi\sqrt{6}}$ $\Rightarrow$ Find σ

$$\boxed{\begin{array}{ll} \ell_E = \sigma\lambda, & B = \sqrt{2\lambda \ell_E} \\ A = \frac{G\lambda^2}{2\pi B}, & \ell_H = \frac{A^2}{3\lambda} \end{array}}$$

PYRAMIDAL HORN

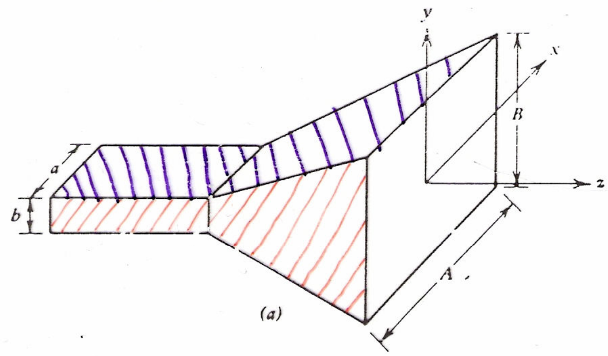

TOP - VIEW

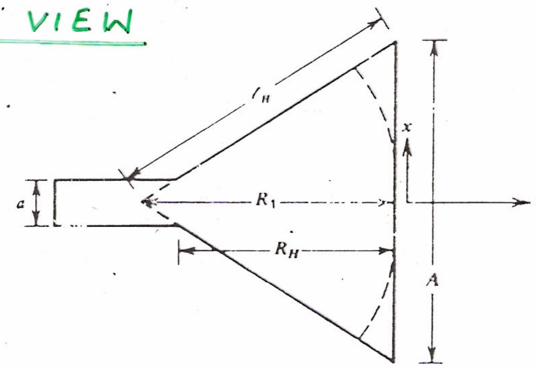

SIDE - VIEW

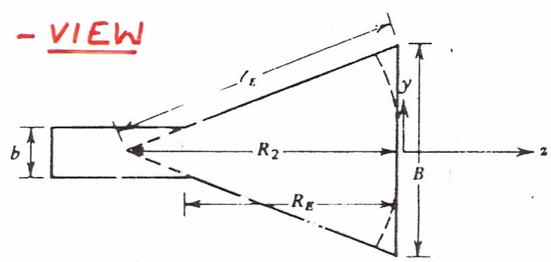

Figure — Pyramidal horn antenna. (*a*) Overall geometry. (*b*) Cross section through the *xz*-plane (*H*-plane). (*c*) Cross section through the *yz*-plane (*E*-plane).

$$\boxed{R_E = R_H}$$

$$E_{ay} = E_0 \cos\left(\frac{\pi x}{A}\right) e^{-j\beta/2\left(\frac{x^2}{R_1} + \frac{y^2}{R_2}\right)}$$

$$D_p = \frac{\pi}{32}\left(\frac{\lambda}{A} D_E\right)\left(\frac{\lambda}{B} D_H\right)$$

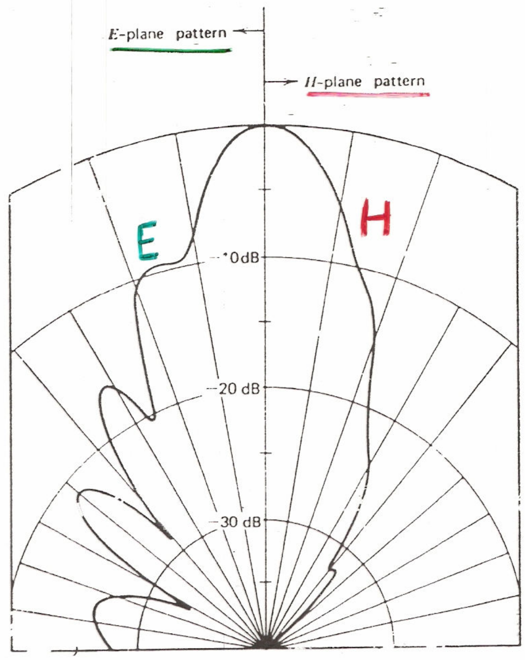

Figure — Principal plane patterns for the optimum pyramidal horn antenna of Example at 9.0 GHz. The patterns include the $(1 + \cos\theta)/2$ factor. $HP_E = 12.0°$ and $HP_H = 13.6°$.

OPTIMUM DIMENSIONS VS. DIRECTIVITY

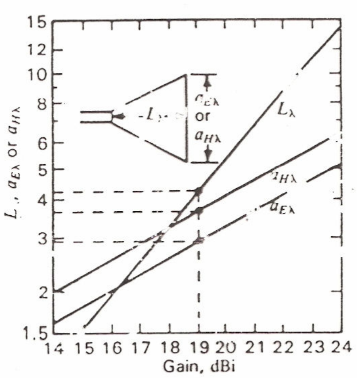

Figure — Dimensions of rectangular (pyramidal) horns (in wavelengths) versus directivity (or gain, if no loss). Thus, noting the dashed lines, a gain of 19 dBi requires a horn length $L_\lambda = 4.25$, an H-plane aperture $a_{H\lambda} = 3.7$ and an E-plane aperture $a_{E\lambda} = 2.9$. These are inside dimensions. It is assumed that δ (E plane) $= 0.25\lambda$ and δ (H plane) $= 0.4\lambda$, making the dimensions close to optimum. It is also assumed that $\varepsilon_{ap} = 0.6$.

OPTIMUM DIMENSIONS VS. DIRECTIVITY

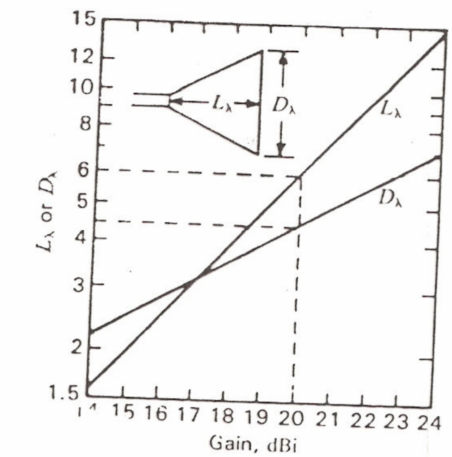

Figure 12 Dimensions of conical horn (in wavelengths) versus directivity (or gain, if no loss). Thus, noting the dashed lines, a gain of 20 dBi requires a horn length $L_\lambda = 6.0$ and a diameter $D_\lambda = 4.3$. These (inside) dimensions are close to optimum.

FIG. 13. Experimentally observed patterns of conical horns of various dimensions.

MULTIMODE HORNS

Diagonal Horn

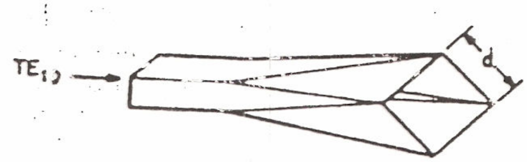

FIG. 14 — Transformation from rectangular waveguide to diagonal horn.

TE_{10} and TE_{01} ⇒ excited with equal amplitude and phase in a square waveguide.

CONICAL HORN

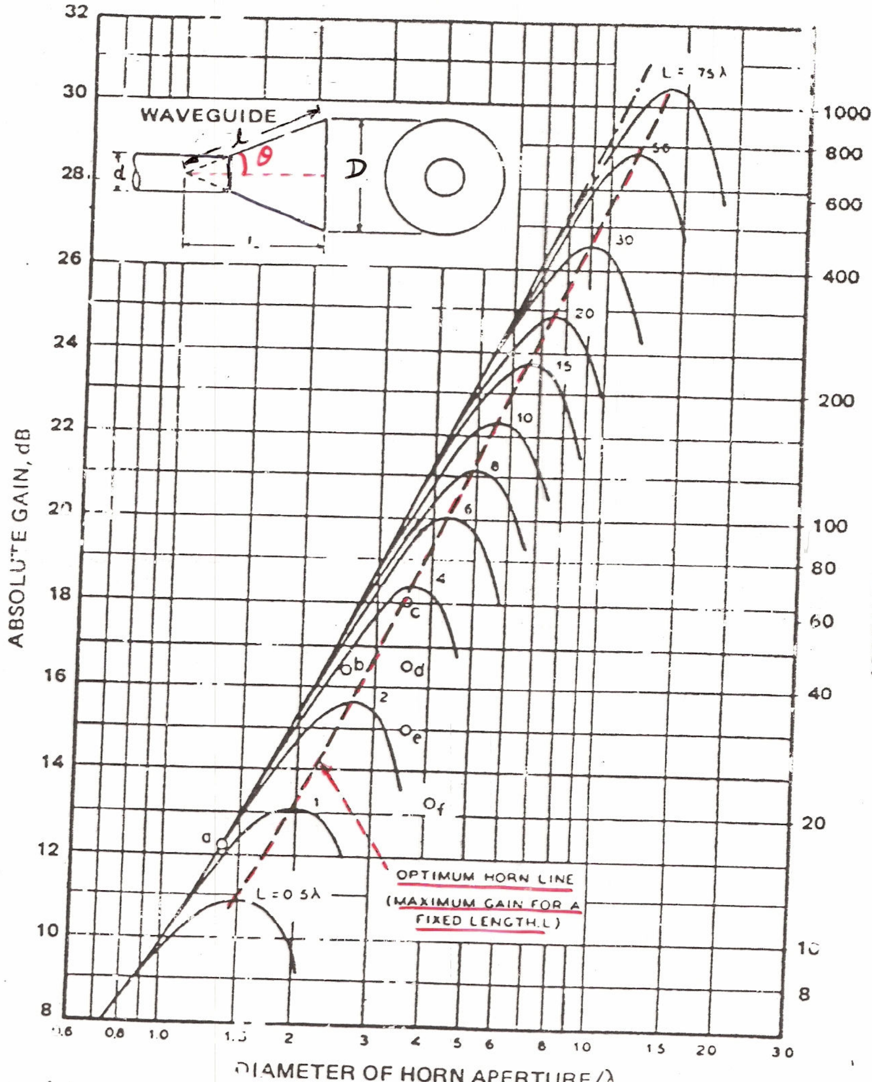

FIG. 11 Calculated gain of a conical horn as a function of aperture diameter with axial length as parameter.

$$\theta = \tan^{-1}\left(\frac{D}{2L}\right)$$

$$S = \frac{D^2}{8\lambda L}$$ = Spherical wave phase error

= 0.30 to 0.375 for optimum gain

GAIN (dB) = 7.0 + 20.6 LOG D/λ

DUAL MODE CONICAL HORN

STEP OF LENGTH l

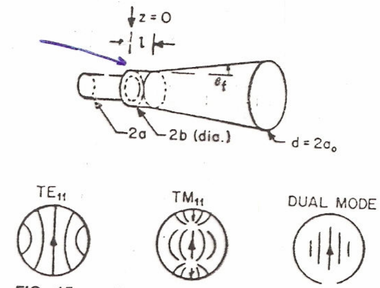

FIG. 15 Dual-mode horn with generating step and its approximate aperture field distribution.

STEP-LESS DUAL MODE HORN

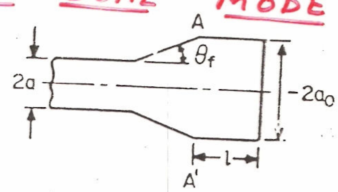

DUAL MODE PYRAMIDAL HORN

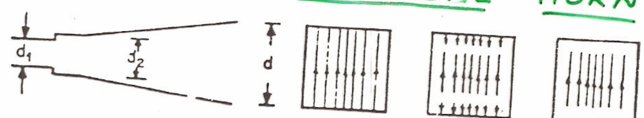

FIG. 17 — Dual-mode pyramidal horn.

FLARE ANGLE CHANGE

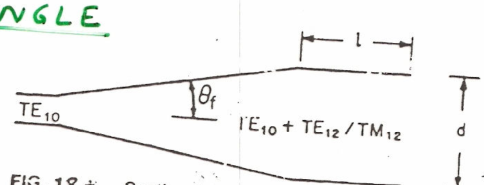

FIG. 18 — Section through square-aperture pyramidal horn with flare-angle change.

Conical Corrugated Horn

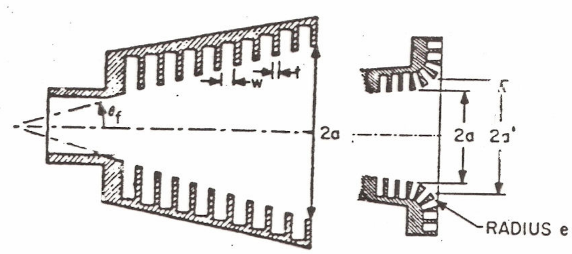

FIG. Small-flare-angle corrugated horn at left; corrugations extended into flange at right.

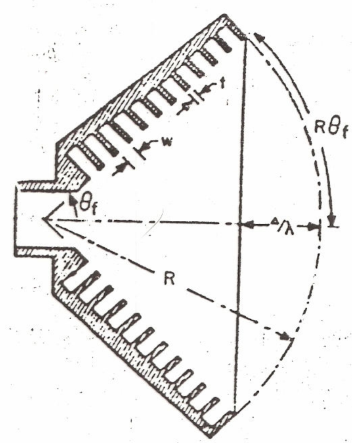

FIG. Wide-flare scalar horn.

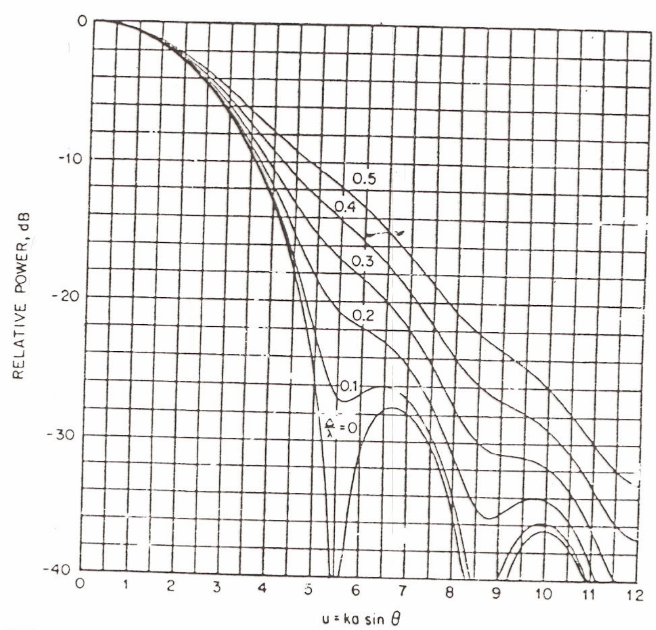

FIG. Universal patterns for small-flare-angle corrugated horns under near-balanced conditions.

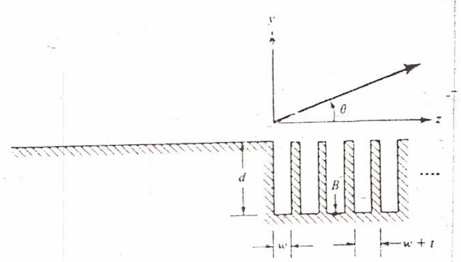

(a) Cor ugated surface

(b) Noncorrugated surface

Geometry of corrugated and plane surfaces.

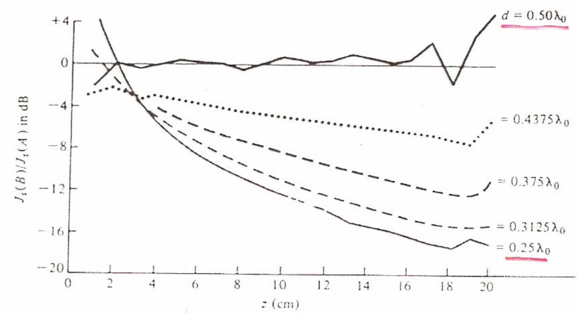

(a) Surface current decay on corrugated surface due to energy forced away from corrugations.

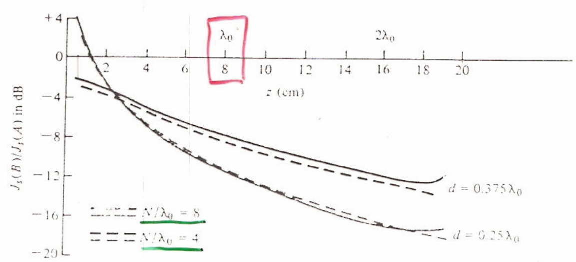

(b) Surface current decay on corrugations as a function of corrugation density.

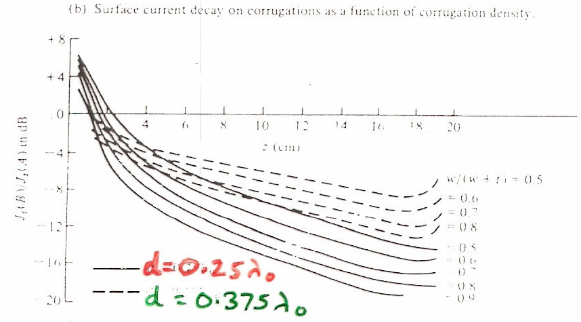

(c) Surface current decay on corrugations as a function of corrugation shape.

Surface current decays on corrugated surface.

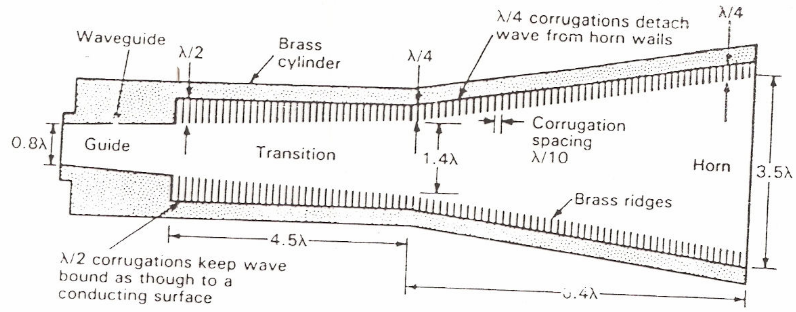

Figure Cross section of circular waveguide-fed corrugated horn with corrugated transition. Corrugations with depth of $\lambda/2$ at waveguide act like a conducting surface while corrugations with $\lambda/4$ depth in horn present a high impedance.

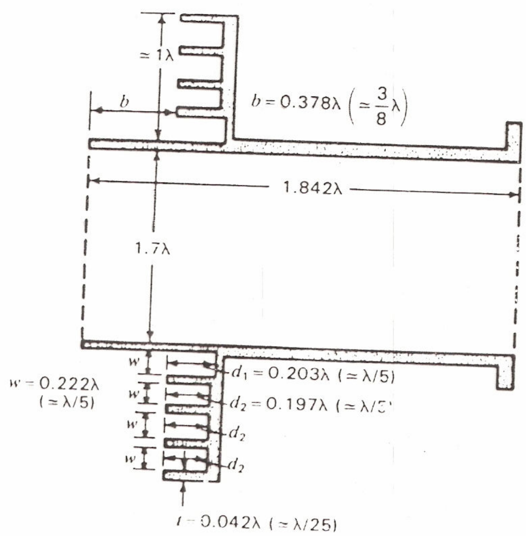

Figure Cross section of circular waveguide with flange and 4 chokes for wide-beam-width high-efficiency feed of low F/D parabolic reflectors.

BROADBAND HORN

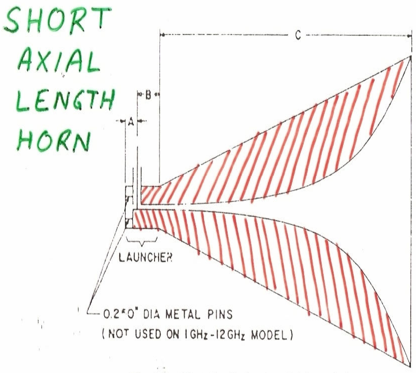

Fig. 19 - Sketch of short axial length horn.

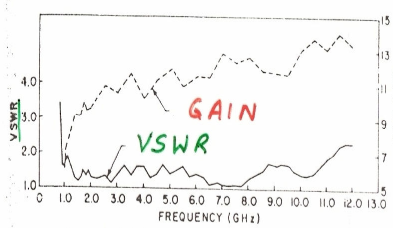

Fig. 20 - VSWR and gain (1.0–12.0 GHz horn).

Table I
Horn Dimensions

Internal Axial Dimensions*		
Dimension	1.0–12.0 GHz-Horn (in)	0.2–2.0 GHz Horn
A	0.325	1.625
B	1.000	5.000
C	6.000	30.0000

Cross Section Dimensions				
Location	Width (in)	Height (in)	Width (in)	Height (in)
Back shorting plate	1.200	0.872	7.000	6.700
Feed point	1.200	0.872	7.000	6.700
Launcher-horn junction	3.400	2.616	14.200	6.700
Horn aperture	9.500	5.440	37.500	27.200

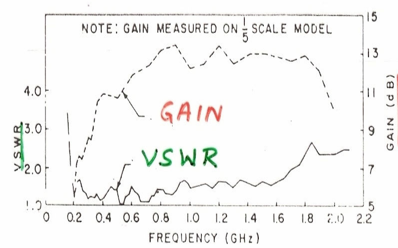

Fig. 21 - VSWR and gain (0.2–2.0 GHz horn).

COMPACT APERTURE MATCHED HORN

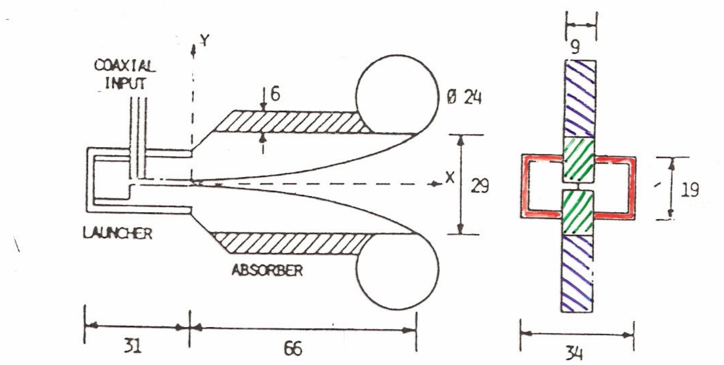

FIG. 22 : A COMPACT, APERTURE-MATCHED ANTENNA

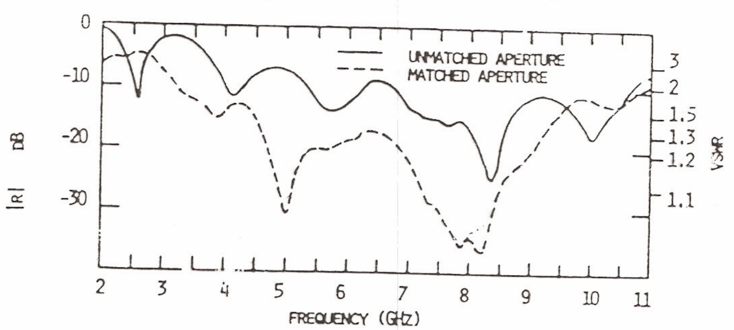

FIG. 23 : MEASURED REFLECTION COEFFICIENT FOR MATCHED AND UNMATCHED ANTENNAS

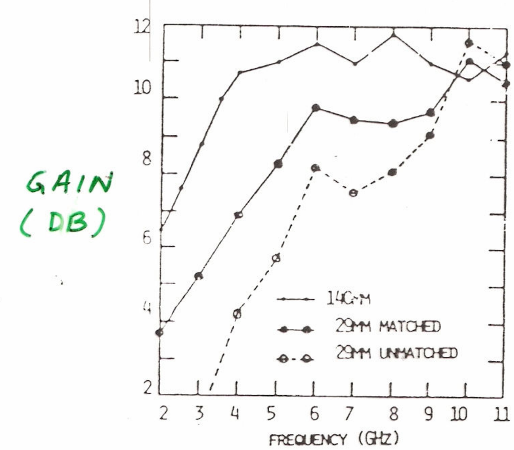

FIG. 24: GAIN OF VARIOUS ANTENNAS